UNIVERSITY OF CALIFORNIA,
IRVINE

Surfactant Enhanced Methane Hydrate Growth in Quiescent Sodium Chloride Solutions

THESIS

submitted in partial satisfaction of the requirements
for the degree of

MASTER OF SCIENCE

in Physics

by

Mason Jackson Eastman

Thesis Comittee:
Professor Peter Taborek, Chair
Professor Derek Dunn-Rankin
Professor Zuzanna Siwy

2016

Contents

List of Figures

Acknowledgement

I would like to thank Peter Taborek for his leadership, Derek Dunn-Rankin and his lab for their collaboration and critiques, my labmates Jeff, David, and Bobby for their support, all my friends in the ChaMP and Physics programs at UCI, and my wonderful family.

Thanks also to the W. M. Keck Foundation for funding this endeavor, and to Academic Press and John Wiley and Sons for allowing the use of their figures.

Abstract of the Thesis

Surfactant Enhanced Methane Hydrate Growth in Quiescent Sodium Chloride Solutions

by

Mason Jackson Eastman

Master of Science in Physics

University of California, Irvine, 2016

Professor Peter Taborek, Chair

Methane hydrate growth was investigated in solutions of between 0 and 10 wt% NaCl in the presence of the surfactants sodium dodecyl sulfate, potassium dodecyl sulfate, and sodium laurate. Total amount of water converted to hydrate and total rate of hydrate formation were both found to greatly decrease with increased NaCl concentration in the presence of all surfactants tested. Different salinity-depenent patterns of growth were observed. Latent heat of hydrate formation was directly measured with deionized water containing sodium dodecyl sulfate. These results could provide a template for a hydrate-based desalination system.

Chapter 1

Introduction

We carried out experiments on the growth of methane hydrates in quiescent (unstirred) systems, from NaCl solutions in the presence of the surfactants sodium dodecyl sulfate (SDS), potassium dodecyl sulfate (KDS), and sodium laurate (NaL). We hoped to use these results as a proof of concept for the desalination of sea water and the high-salinity byproducts of hydraulic fracturing. Focusing on quiescent systems eliminates the need for expensive and energy-intensive stirring apparatus. Others have investigated hydrate growth kinetics with NaCl solutions in porous media,[1, 2] as well as the kinetics of systems with surfactants but without NaCl [3, 4, 5] and the thermodynamics of NaCl solutions.[6, 7, 8]

Gas hydrates are a specific type of clathrates — a class of compounds consisting of 'cages' of one molecule enclosing and stabilized by a different 'guest' molecule — in which the cages are formed by hydrogen-bonded water, and the guests are formerly-dissolved gas molecules.

1.1 History

Gas hydrates were first synthesized in the laboratory by Humphry Davy in 1810, as part of his experiments with oxymuriatic acid (chlorine gas).[9] These experiments were later confirmed by Davy's assistant Michael Faraday, who also determined the ratio of H_2O to Cl_2 to be 10 to 1.[10] In these early days gas hydrates were regarded as an interesting curiosity, but had few practical applications.

Research on clathrate hydrates continued throughout the 19th and early 20th centuries, but in 1934 E. G. Hammerschmidt made a major discovery that brought this research into the mainstream.[11] He found that the snow-like buildup which commonly blocked natural gas pipelines was composed of hydrates of various combinations of methane, ethane, propane, and isobutane rather than simply frozen water. Subsequently, the natural gas industry commissioned a huge amount of research into hydrate inhibition. Inhibition became a very important economic problem: By 1995, the natural gas industry spent more than $500,000,000 annually on methanol injection alone as a hydrate prevention measure.[12]

1.2 Geometry

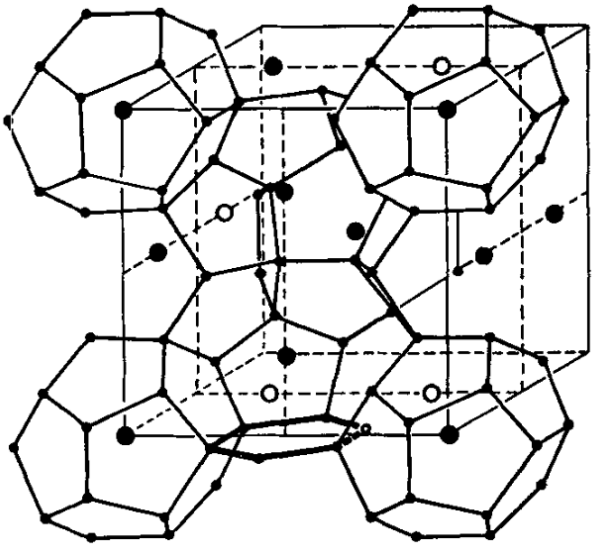

Figure 1.1: A unit cell of Structure I. Large dots represent the centers of the two types of cages. Reprinted with permission from "Clathrate Solutions," by J. H. van der Waals and J. C. Platteeuw, 1959, *Adv. Chem. Phys., Volume 2*, p. 7.[13] Copyright 1959 by John Wiley and Sons.

There are three major known configurations of hydrate cages. These will form depending on various properties of the guest molecule, the most important being molecular size. Both structure I (sI) and structure II (sII) configurations feature 5^{12} dodecahedra, but they are joined differently. sI, shown in Figure 1.1, also includes $5^{12}6^2$ 14-hedra (polyhedra with 12

pentagonal sides and two hexagonal ones) whereas sII includes $5^{12}6^4$ 16-hedra.[14] Although sI and sII structures were formalized in the 1950's [15], a third major configuration called structure H (sH) was discovered in 1987.[16] sH hydrates require a mixture of small and large guest gases to be stable, and are much less seen.

1.3 Surfactants

Surfactants are molecules most often employed in soaps and detergents which contain both a hydrophilic 'head' and a lipophilic (also hydrophobic) 'tail'. When dissolved in water, an amount of surfactant molecules tend to adsorb at the water-gas interface, with the tail outside of the water and the head remaining submerged. Thus a single layer of surfactant molecules forms at the surface (Figure 1.2). Because the tails are nonpolar, if the gas above this interface is nonpolar as well, the dissimilarity at the interface is reduced and the surface tension is lowered.

In quiescent (unstirred) systems of liquid water and gaseous methane, like those explored here, surfactants are vital to hydrate growth. In the absence of surfactant, a thin layer of clathrate will grow on the boundary between water and gas, completely covering the water's surface without holes and isolating the gas from the water. Although this layer will continue to thicken and grow upward,[17] the rate of growth is so small as to be negligible for practical purposes and the bulk of the water will not form hydrate. Surfactants are thus necessary in qui-

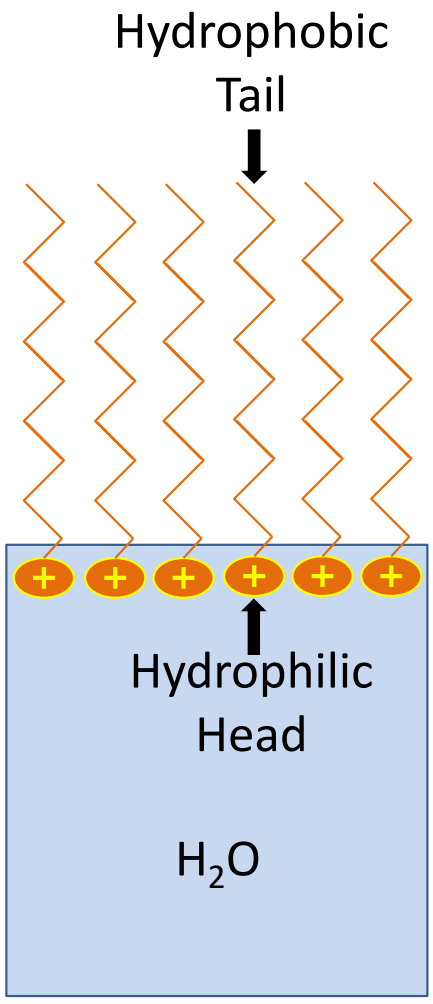

Figure 1.2: A single layer of surfactant at the water-gas interface.

escent systems to achieve high hydrate growth rates for viable industrial processes.

In the presence of large enough concentrations of certain surfactants, notably SDS (sodium dodecyl sulfate) in methane systems, this unbroken layer does not form. Instead, hydrate crystals cling to the walls of their container and gradually climb up it at a roughly constant rate. In so doing, the area of contact between the liquid water and gas layers is constantly renewed.

1.4 Inhibition

Following Hammerschmidt's seminal 1934 paper, gas hydrate inhibition became a very important and popular topic. Many methods have been employed, including injection of methanol and ethylene glycol. Many salts, including sodium chloride, also act as thermodynamic inhibitors of hydrate growth. They shift the hydrate-containing portion of the water-methane phase diagram toward lower temperature and higher pressure (Figure 1.3).[6] This is due primarily to coulombic forces from the dissolved ions attracting water molecules, making it more difficult for them to form crystals. Secondarily, the dissolved ions "salt out" hydrate-forming units, limiting their solubility.

Whereas generally salts are employed to prevent hydrate nucleation, we have focused on the properties of hydrates that nonetheless form under altered temperature and pressure conditions. Additionally, we have tested the underexplored interactions between hydrate promotors (surfactants) and inhibitors (salt).

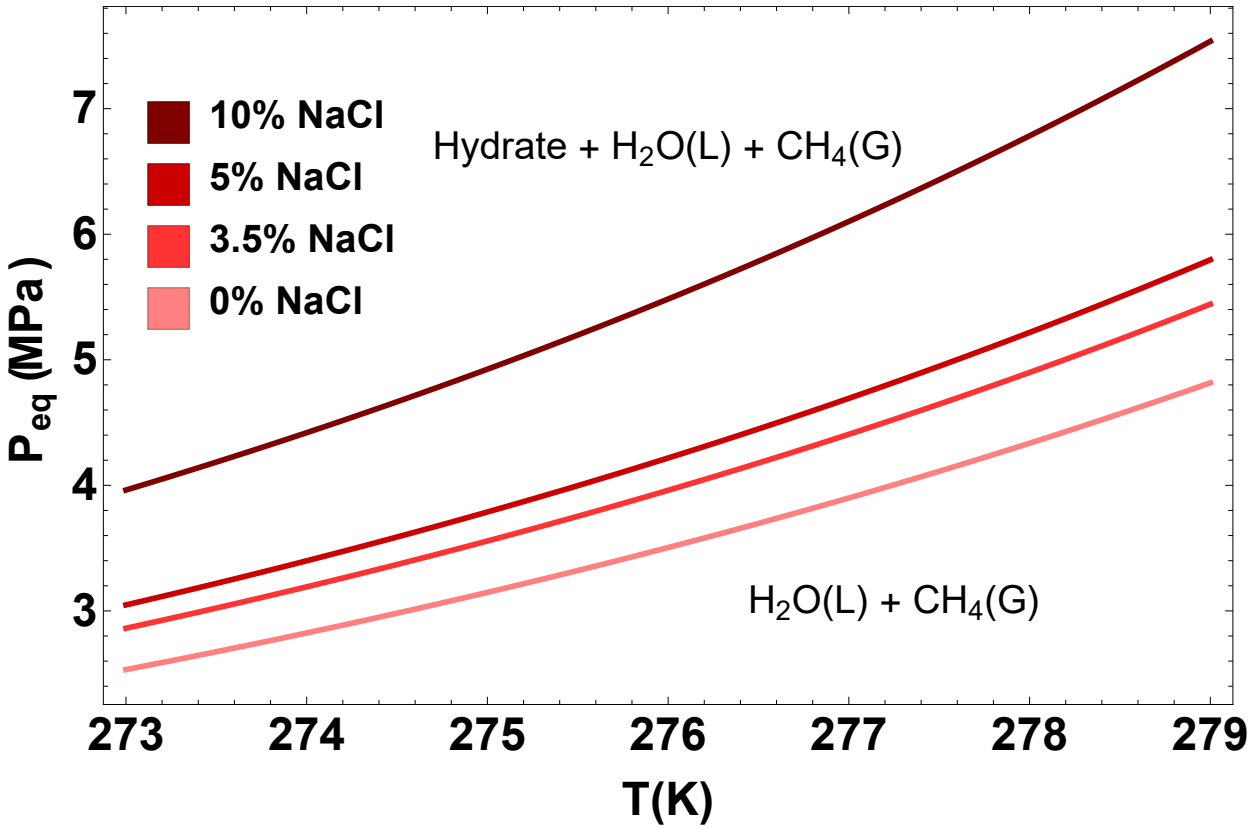

Figure 1.3: The equilibrium line between liquid-gas and hydrate-liquid-gas of a H_2O-CH_4-NaCl system for different salt concentrations, from a fit to experimental data by De Roo et al.[6]

Chapter 2

Theory

2.1 Hydration Number

Because its size falls between 4.2Å and 6Å, pure methane will form sI hydrate. When reduced to a perfect unit cell, this structure contains 1 methane molecule for every 5.75 water molecules. This is called the maximum theoretical hydration number N_h, and gives an upper limit to the amount of methane that can be absorbed and converted to hydrate. This is based on a model proposed by Van der Waals and Platteeuw,[13] which assumes a uniformly solid hydrate structure. With this assumption, N_h can be derived through geometry: In sI hydrates, for every 1 molecule of water there are $\nu_{small} = {}^{1}\!/_{23}$ and $\nu_{large} = {}^{3}\!/_{23}$ small and large cavities, respectively. The hydration number N is then given by

$$N = \frac{1}{\nu_{small}\theta_{small} + \nu_{large}\theta_{large}} \tag{2.1}$$

where the θ's are the occupancies of the small and large cavities. The chemical makeup is then $(CH_4 \cdot \mathrm{N}H_2O)$. When all cages are filled, $\theta_{small} = \theta_{large} = 1$ and we get the maximum hydration number

$$N_h = \frac{1}{v_{small} + v_{large}} = \frac{1}{{}^{1}\!/_{23} + {}^{3}\!/_{23}} = 5.75 \tag{2.2}$$

To a better approximation, N_h varies with pressure and temperature. It can be deter-

mined accurately by simulation programs such as CSMGem, which uses Gibbs free energy minimization techniques and does not assume uniform solid structure. CSMGem uses an iterative algorithm developed by Ballard and Sloan[18], which first assumes temperature equilibrium, pressure equilibrium, and equal fugacity for all phases in the system. It next posits an equation guaranteeing mass balance for all phases, and an equation for phase composition of all phases. Once these are set up, the algorithm sets a series of parameters to initially estimated values. It then cycles through a loop of incrementally increasing or decreasing these parameters, and checking for completion. The procedure is complete when the Gibbs free energy is minimized (determined by the mass balance equation totaling to zero) and the change in composition of each phase is zero.

2.2 Surfactant Effects

Although it is well-established that surfactants promote the growth of methane hydrates,[3, 5, 19, 20] the reasons for this are still not well understood. Surfactants' tendency to form micelles (spherical suspensions with hydrophilic 'heads' pointing outward, and hydrophobic 'tails' pointing inward) has been shown not to be responsible.[19, 21, 22, 23] The primary evidence against this theory has been the observed growth of hydrates in quiescent systems through the use of surfactants at significantly less than the critical micelle concentration (CMC), above which micelles form.

It has been theorized[22, 23] that surfactants prevent agglomeration of hydrate units. Instead of forming a solid barrier across the water-gas interface, units in the presence of surfactants move apart. They form a crystallization front which moves up the walls of their container, probably due to capillary forces (although this has not been confirmed experimentally). This leaves the water-gas interface unobstructed, and the moving water-surfactant solution carries hydrate units created at the interface up the walls. Thus hydrate formation proceeds unimpeded, and at a significantly higher rate and to a higher percentage

of the theoretical maximum compared to a system without surfactant, since it is no longer confined to the surface of the water.

2.3 Hydrate Growth

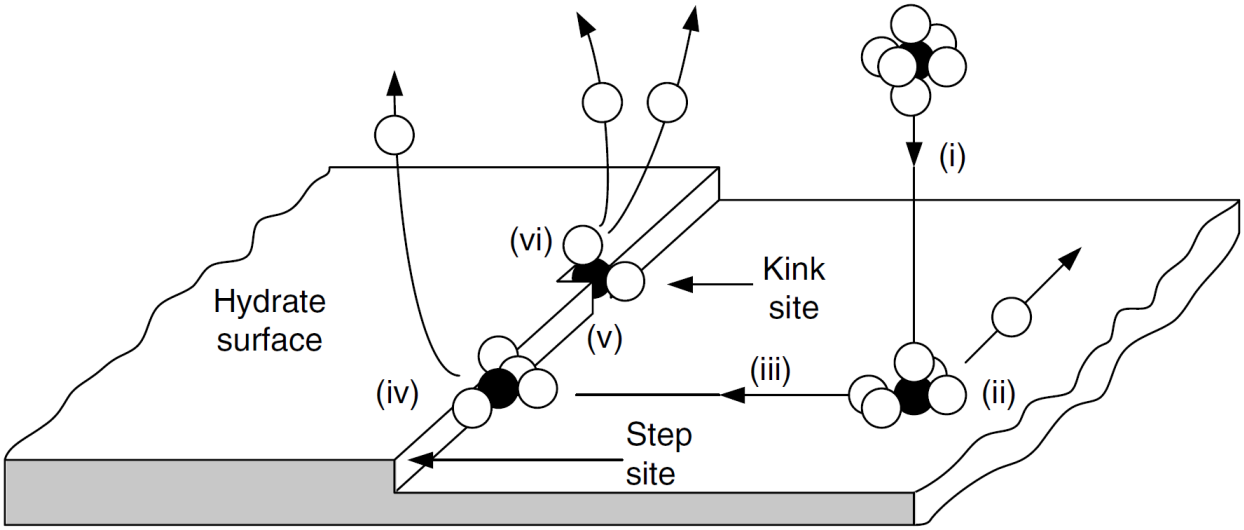

Figure 2.1: Steps of hydrate crystal growth. Reprinted with permission from Sloan Jr, E. Dendy, and Carolyn Koh. *Clathrate hydrates of natural gases*. CRC press, 2007. Modified from Elwell, D., Scheel, H.J. *Crystal Growth from High Temperature Solutions*. Copyright Academic Press, 1975.

The growth of hydrate crystals can be conceptually understood as a filling, one 'unit' at a time, of a flat surface.[24] The units in this picture are short-lived water hydration cells surrounding a guest gas molecule.[25] This filling takes several actions, alternately costing and releasing energy (Figure 2.1). First, the unit will transport to the crystal surface (i), and adsorb onto the surface (ii). Next the unit will transport across the surface (iii) and attach to a 'step' (iv) - a portion of the surface which is raised one unit above. Since it will be in contact with two surfaces instead of one, this is energetically favorable for the unit. Next the unit will diffuse across the step (v), and be integrated into a 'kink' in the step (vi) - a portion without an existing unit. Since there are three contact surfaces there, this is the most favorable position for the unit.

Englezos et al.[26] developed a quantitative theory of hydrate growth rates in 1987. Growth rates in this model are proportional to a 'driving force' given by the fugacity difference of the guest gas from three-phase (L-G-H) equilibrium:

$$R(t) = K(f - f_{eq}) \tag{2.3}$$

$R(t)$ is the growth rate, K is a parameter which depends upon various properties of the system (including interfacial area), and f is the methane's fugacity. Fugacity is proportional to pressure, and is equal for an ideal gas. In a high pressure system such as ours, which obeys a real gas law, some modification is required:

$$f = \phi P \tag{2.4}$$

$$\ln \phi = \int_0^P \frac{Z(P', T) - 1}{P'} \, dP' \tag{2.5}$$

$Z(P, T)$ is the compressibility factor at a given pressure and temperature, and ϕ is the fugacity coefficient. For an ideal gas, $\phi = 1$.

2.4 Real Gas Law

Under conditions close to standard temperature and pressure, the ideal gas law would be used to calculate the moles of methane gas converted to hydrate. However, due to the high pressures (> 50 atm) required for methane clathration, a real gas law was required. The Peng-Robinson equation of state[27] is most commonly used for this purpose. It is a method for determining a compressibility factor, Z, for use with the real gas equation $PV = nRTZ$. First, two values are calculated:

$$A = \frac{0.457235 P T_c^2}{P_c T^2} \left(1 + \kappa \sqrt{T/T_c}\right)^2 \tag{2.6}$$

$$B = \frac{0.077796 P T_c}{P_c T} \tag{2.7}$$

where $P_c = 4.5922$ MPa is the critical pressure and [28] $T_c = 190.564$ K is the critical temperature of methane, and $\kappa = 0.37464 + 1.54226\omega - 0.26992\omega^2$ is a constant derived from methane's acentric factor $\omega = 0.01141$.[29] From there, the compressibility factor, Z, can be determined by solving the polynomial equation

$$Z^3 - (1 - B)Z^2 + (A - 3B^2 - 2B)Z - (AB - B^2 - B^3) = 0 \tag{2.8}$$

Z can be calculated for each P-T measurement, and used to calculate the moles of gas present through

$$n = \frac{PV}{RTZ} \tag{2.9}$$

2.5 Latent Heat

Like water freezing, the formation of gas hydrates is an exothermic process. The energy released during that formation, and thus the latent heat of formation, can be determined through calorimetry. This value is important to assessing the viability of hydrate formation as a desalination procedure. Assuming only convective heat transfer, the temperature change of one system in thermal contact with another is governed by

$$\frac{dQ(t)}{dt} = mc\frac{dT_w(t)}{dt} = \alpha(T_w(t) - T_g(t)) + \frac{dQ_L(t)}{dt} \tag{2.10}$$

where $T_w(t)$ is the temperature of the water/beaker system, $T_g(t)$ is the temperature of the gaseous methane, mc is the combined mass times heat capacity of the water-beaker system, $Q_L(t)$ is the heat released by hydrate formation, and α is a coupling constant between the two systems, which can be determined experimentally.

In order to take the derivative of the water's temperature, we applied a Savitzky-Golay

filter. This filter's main purpose is smoothing: It generates a set of convolution coefficients based on a least-squares fit method, then multiplies adjacent points in a dataset by these coefficients, adds them up and divides by a normalization factor. This behaves similarly to a moving average. As stated by Savitzky and Golay in their 1964 paper,[30]

$$Y_j^* = \frac{\sum_{j=-m}^{j=m} C_i Y_{j+i}}{A} \tag{2.11}$$

where C is the set of convolution coefficients, Y is a data point, m is the number of points to be considered on either side, and A is a normalization factor. A derivative of the smoothed dataset can be developed from this procedure by taking the derivative of the polynomial least-squares fit, and altering the convolution coefficients accordingly. Derivatives of degree D also introduce an additional factor of ${}^{D!}/_{(\Delta t)^D}$:

$$\frac{d^D Y_j^*}{dt^D} = \frac{D!}{(\Delta t)^D} \frac{\sum_{j=-m}^{j=m} C_i' Y_{j+i}}{A} \tag{2.12}$$

Latent heats can be predicted by the Clapeyron equation[31], which relates the analogous quantity of enthalpy change during a state transition to the slope of the pressure-temperature curve.

$$\frac{dP}{dT} = \frac{\Delta H}{T \Delta P} \tag{2.13}$$

Chapter 3

Experimental Procedure

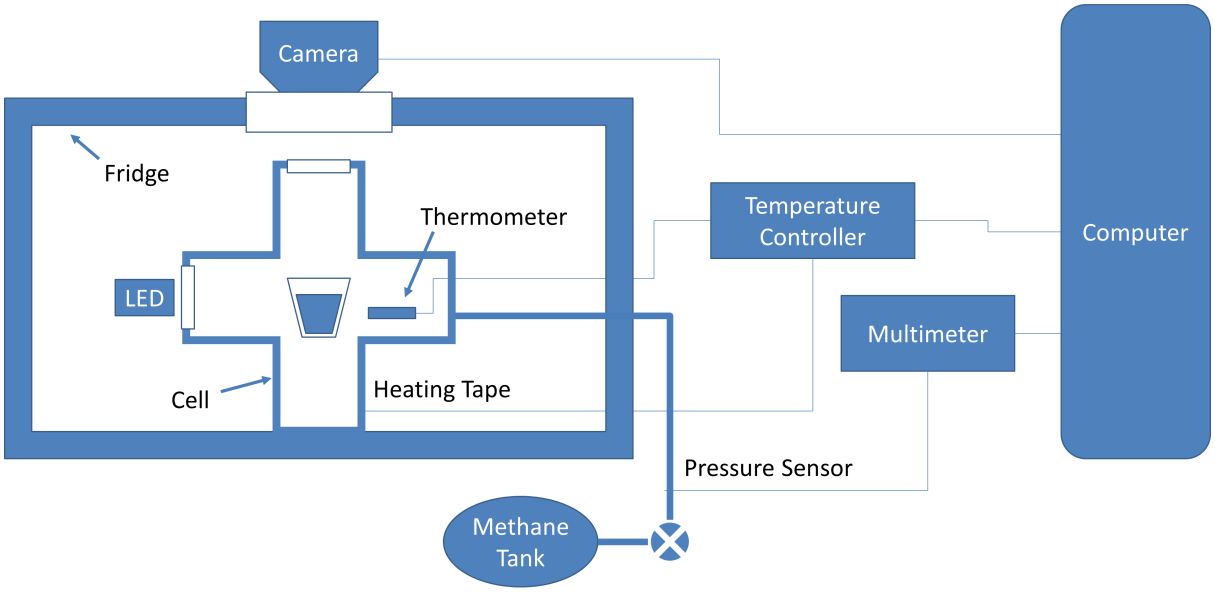

Figure 3.1: A diagram of the experimental setup

For each trial a total of 40 grams of deionized water, non-iodized table salt, and surfactant (Sodium Dodecyl Sulfate, Potassium Dodecyl Sulfate, or Sodium Laurate) were mixed in a glass beaker. This was placed in a ∼1.67L commercial schedule 80 steel cross pipe from Gruvlok (henceforth known as the "pressure cell"), equipped with two $^{5}/_{8}$-inch thick sapphire windows for viewing and allowing in light from an external LED. There were two different setups, both represented by Figure 3.1 and identical except for a few minor differences. One had its cell standing vertically, with its beaker supported by a teflon 'table'. Due to the

shape of its fridge, the other setup's cell was horizontal, with a slightly shorter and wider beaker loaded from the side.

Before each run, the pressure cell was opened and thoroughly dried. The glass beaker was taken out, rinsed with deionized water and dried. The cell with glass beaker inside was then placed inside a custom-built optical refrigerator. A gas line connected the cell to a tank of 99.5% purity methane supplied by Airgas.

The methane pressure was brought to 50 psi ($\approx$ .34 MPa) and then flushed three times in order to remove the air from the cell. Then the pressure was increased to a level such that it would decrease to a target pressure when the cell had cooled isochorically to a target temperature. Once it reached this level, the cell was isolated by a valve. These target pressures and temperatures varied depending on the NaCl concentration of the water, with higher concentrations generally requiring higher pressures and/or lower temperatures. In order to be well within the clathrate-forming region of the phase diagram, we picked pressures $\sim$250 psi higher than the equilibrium point, determined based on an experimental fit from De Roo et al.[6] We used still higher pressures for some runs.

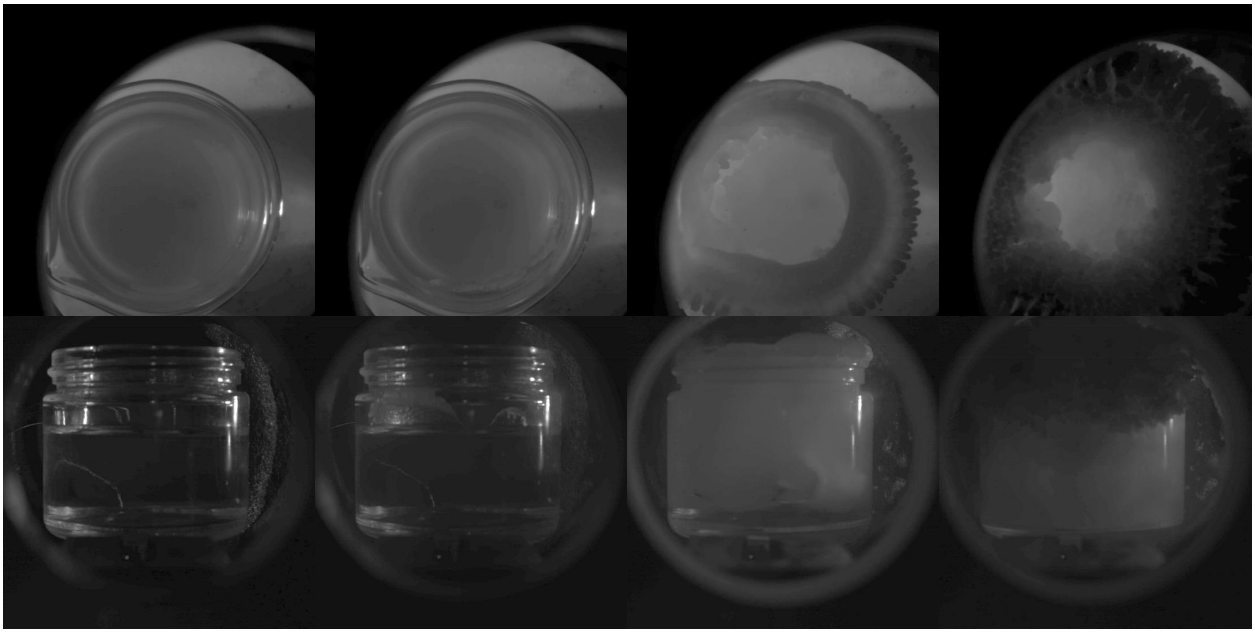

Figure 3.2: Typical progression of low-salt clathrate growth. Top is the vertical cell, bottom is horizontal.

Pictures were then taken at regular intervals with a Nikon D5200 digital camera. These were used to visually identify the start of hydrate formation, defined as the first appearance of hydrate crystals as seen in the second panels of Figure 3.2. Images were variously captured from the top and from the side, with light provided through the other window by an LED. The camera was covered with a black cloth to eliminate excess light.

Pressure was measured by an Omega PX309 pressure gauge. Temperature was measured using a 100Ω Omega platinum RTD thermometer, read via 4-wire methods by a Stanford Research Systems CTC100. This same device maintained a PID temperature loop using heating tape wrapped around the outside of the cell. Pressure and temperature were constantly measured with a LabView program.

3.1 Gas Amount Calculation

Using the Peng-Robinson equation of state, values of Z were calculated for use with the real gas equation $PV = nRTZ$. From this, the number of moles of methane gas in the cell could be calculated. The maximum number of moles of methane that could be converted to hydrate would therefore be:

$$n_{abs,max} = \frac{m_w}{M_w N_h} \approx \frac{40 \text{ g}}{18.015 \text{ g/mol} \times 5.75} = 0.386 \text{ mol} \tag{3.1}$$

Where m_w is the mass of the water used, M_w is the molar mass of water, and N_h is the maximum hydration number (which varies with pressure and temperature, but can be approximated as 5.75 for sI hydrates). Thus the percentage absorbed could be calculated at any time by taking the difference between the current number of moles of methane and the number of moles at the start of clathration, dividing by the theoretical maximum, and multiplying by 100%.

$$p_{abs} = \frac{n_{0,CH_4} - n_{CH_4}}{n_{abs,max}} \times 100\% \tag{3.2}$$

$$n_{CH_4} = \frac{PV}{RTZ}$$

$$n_{0,CH_4} = \frac{P_0 V}{RT_0 Z_0}$$

The maximum gas converted to hydrate was determined by a Mathematica program. It calculated the maximum rate of gas consumption and then defined complete clathration as the point at which the rate was 20% of that maximum. This method was also used by Okutani et al.[5] in determining maximum methane uptake.

3.2 Latent Heat Measurement

We measured the latent heat of methane hydrate formation with almost the exact same setup, with 40 mL of deionized water dissolving 2000 PPM of sodium dodecyl sulfate. However, we now measured two temperatures: That of the gas in the cell as before, and that of the water in the beaker. To measure the water temperature and ensure rapid temperature response, we attached a large coil made from copper shim stock to another 100Ω Omega platinum RTD thermometer, and placed it in the water.

In order for Equation 2.10 to apply to this situation, we had to separate out the mc term to represent all parts of the beaker-water system. We also had to account for the fact that the heat capacity of the water would change as it became hydrate, and made the minor simplifying assumption that initial water mass and maximum hydrate mass were the same. The equation then becomes:

$$\frac{dQ_L(t)}{dt} = (m_w\{(1 - p_H(t))c_w + p_H(t)c_H\} + m_c c_c + m_b c_b)\frac{dT_w(t)}{dt} - \alpha(T_w(t) - T_g(t)) \quad (3.3)$$

where m_w, m_c, and m_b are respectively the masses of the water, copper coil, and beaker; c_w, c_H, c_c, and c_b are the specific heat capacities of water, methane hydrate, copper, and glass; and $p_H(t)$ is the fraction of water converted to hydrate at a given time.

Chapter 4

Results and Discussion

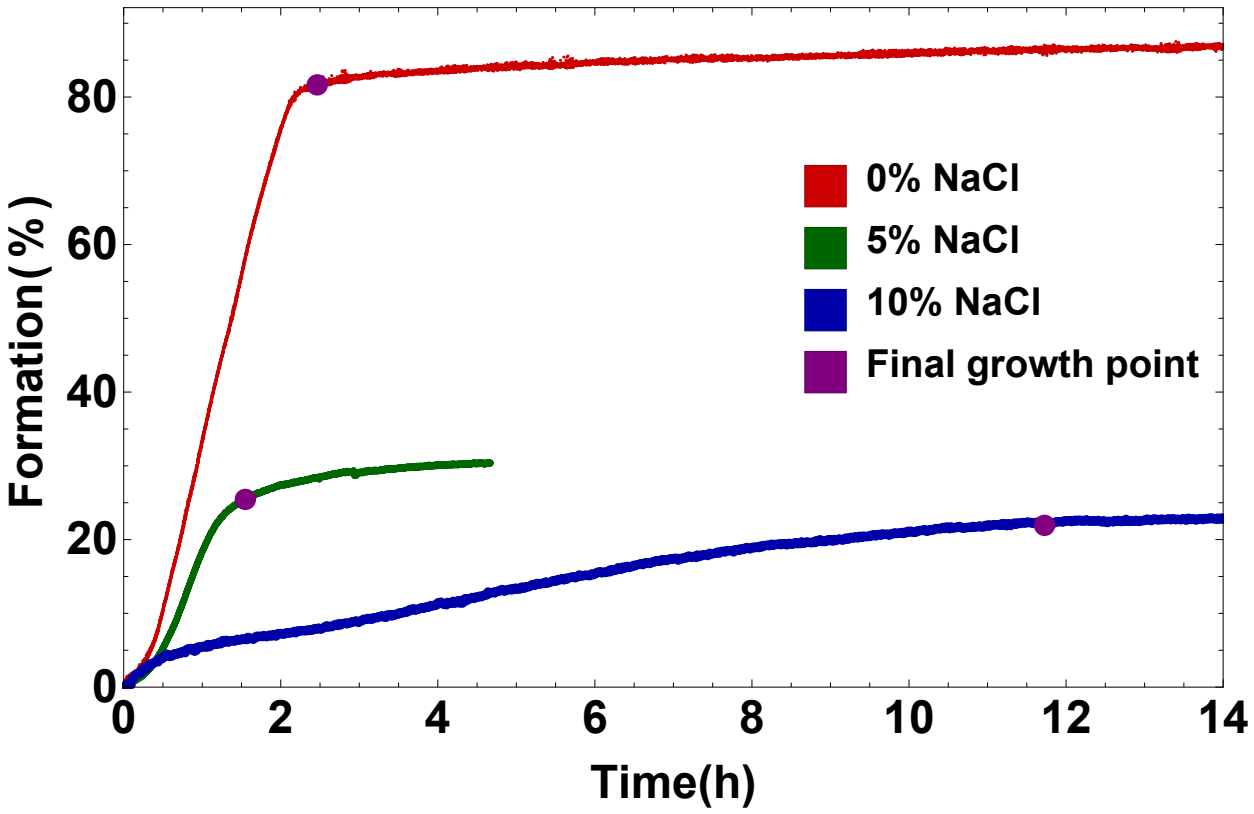

Figure 4.1: Typical growth curves for low and high concentrations of NaCl

After pressurizing, all samples used followed the same basic pattern (Figure 4.1). First, there was a variable amount of 'induction time' during which the hydrate nucleated and the amount of absorbed methane remained roughly constant. Once nucleation occurred (determined by the first appearance of visible hydrate in pictures), there was a brief 'ramp-

up period' of accelerating absorption rate. After that there was a period of linear gas absorption which made up the bulk of the growth, and which we record as the maximum growth rate. Finally, the absorption rate slowed to nearly (but not necessarily exactly) zero.

4.1 Total Absorption

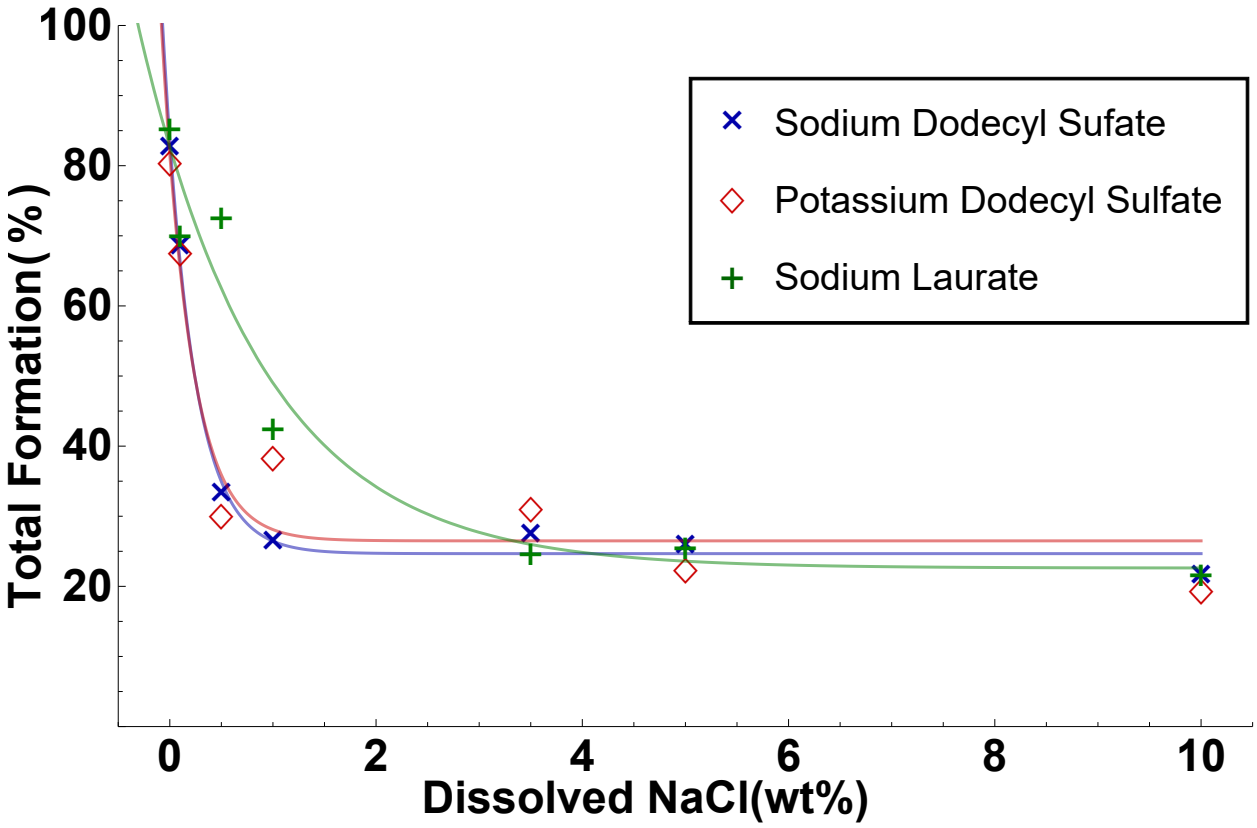

Figure 4.2: Average final methane absorption percentage as a function of water salinity for all three surfactants

Figure 4.4 shows the per-surfactant average of total growth, as defined by Equation 3.2, at different water salinities. We used a hydration number of $N_h = 5.75$ for all measurements. We observed an immediate, precipitous drop in the final percentage of methane absorption with increased salinity for water containing the surfactants sodium dodecyl sulfate (SDS) and potassium dodecyl sulfate (KDS). Water containing sodium laurate (NaL) decreased in final percentage more gradually, notably out-performing SDS and KDS at 0.5% and 1%

NaCl concentration. All three became nearly equal at higher salinities, however, with final absorption percentages at 10% NaCl concentration of 21.6%, 19.5% and 22.0% for SDS, KDS, and NaL respectively. Exponential fits of the form $p = a + be^{-cx}$ — where p is the total formation percentage and x is the salinity — agreed closely with data, with R^2 values of 0.997, 0.973, and 0.984 respectively.

4.2 Growth Patterns

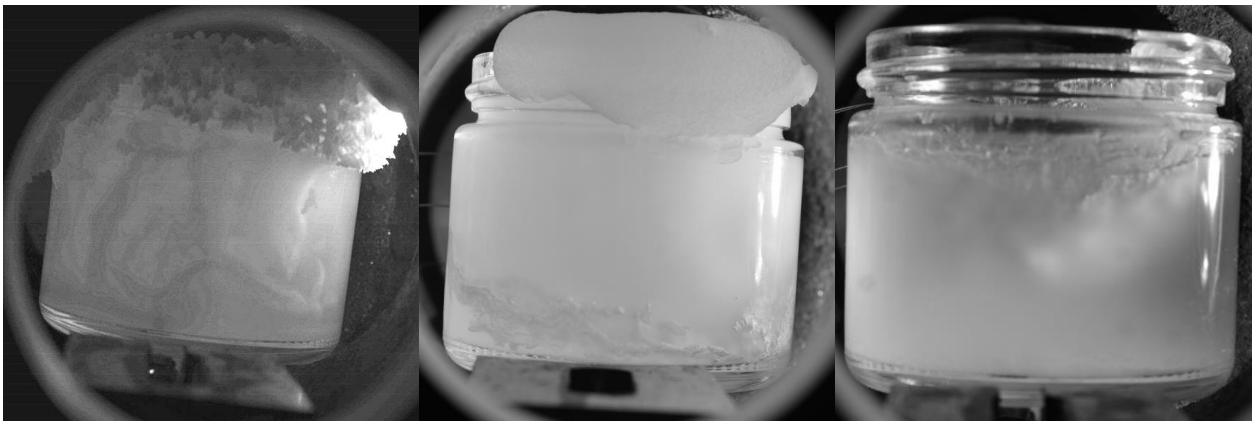

Figure 4.3: Three fully-grown hydrate samples. From left to right: 0 wt% NaCl, 1 wt% NaCl, and 10 wt% NaCl.

We observed three distinct visible patterns in our hydrate growth (Figure 4.3), depending on the salt concentration of the water. At very low salinity, especially 0 wt%, we saw 'dendritic' growth. This was categorized by a rough, thick crystalline layer climbing up the sides of its container. At medium salinities, generally from 1 wt% to 5 wt%, we saw a similar growth pattern with the hydrate climbing up the walls, leaving a basin in the middle. Unlike the dendritic growth, the surface of this hydrate was mostly smooth, and it achieved less height. At 10 wt% and sometimes 5 wt%, we observed a third growth pattern in which a thin layer of hydrate coated the walls of the container initially, but the bulk of growth appeared to happen directly on the horizontal water-gas interface.

4.3 Growth Rate

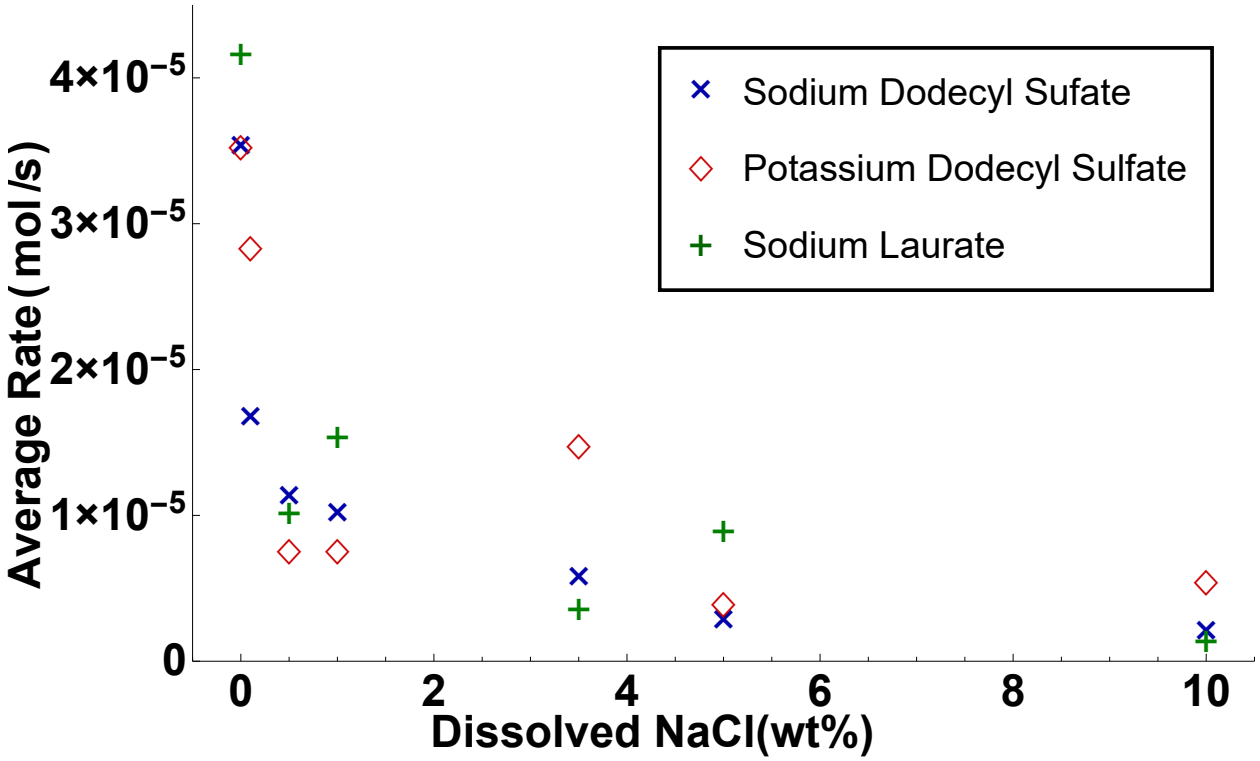

Figure 4.4: Average maximum hydrate growth rates at different salinities

Raw, averaged measurements of maximum rates of hydrate growth (Figure 4.4) show a clear trend toward slower growth at higher NaCl concentrations. Unlike with total growth amount, there is no clear lower limit to this decrease.

Not all of our samples reached their target temperature after being pressurized. Some had a short enough induction time that they began forming hydrate at a higher temperature. In order to correct for the differences in starting points of different samples, we normalized the results (Figure 4.5) by dividing each rate by the relative fugacity $f - f_{eq}$ at the beginning of growth. Additionally, we eliminated samples with less than 40 mL of liquid volume. Because hydrate climbs the walls of the beaker and creates additional water-gas interface, these samples in smaller beakers had an interfacial area that was inconsistent, difficult to quantify, and analysis of which was outside the scope of this experiment.

In this normalized form, the trend of near-immediate drop in growth rate with increased

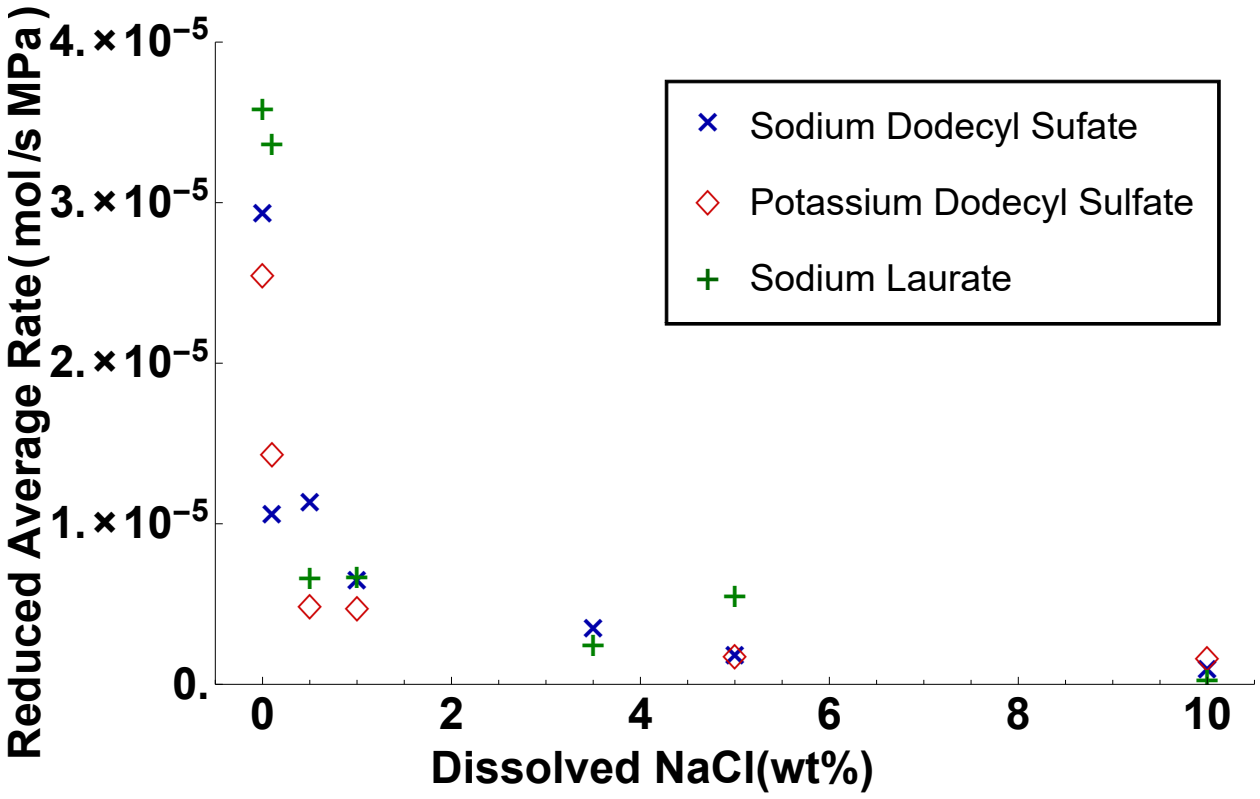

Figure 4.5: Average initial rates of hydrate growth divided by the driving force, $f - f_{eq}$, at different salinities

salinity is more pronounced. At 1 wt% NaCl concentration, the growth rates of samples containing SDS, KDS, and NaL have decreased to 22%, 19%, and 19% respectively of their values without NaCl. NaL seems to outperform the other surfactants at low NaCl concentrations in growth rate as well as total formation.

4.4 Latent Heat of Formation

We determined the value of the coupling constant α from Equation 2.10 by analyzing an early time in the cooldown of the system, before the heating tape had turned on or hydrate formation had begun, such that there were no additional sources of power. For measured values of T_w, T_g, and ${}^{dT_w}/_{dt}$, we found an α value of $-0.57{}^{W}/_{K}$.

As expected, we observed a large spike in the water's temperature slightly after the

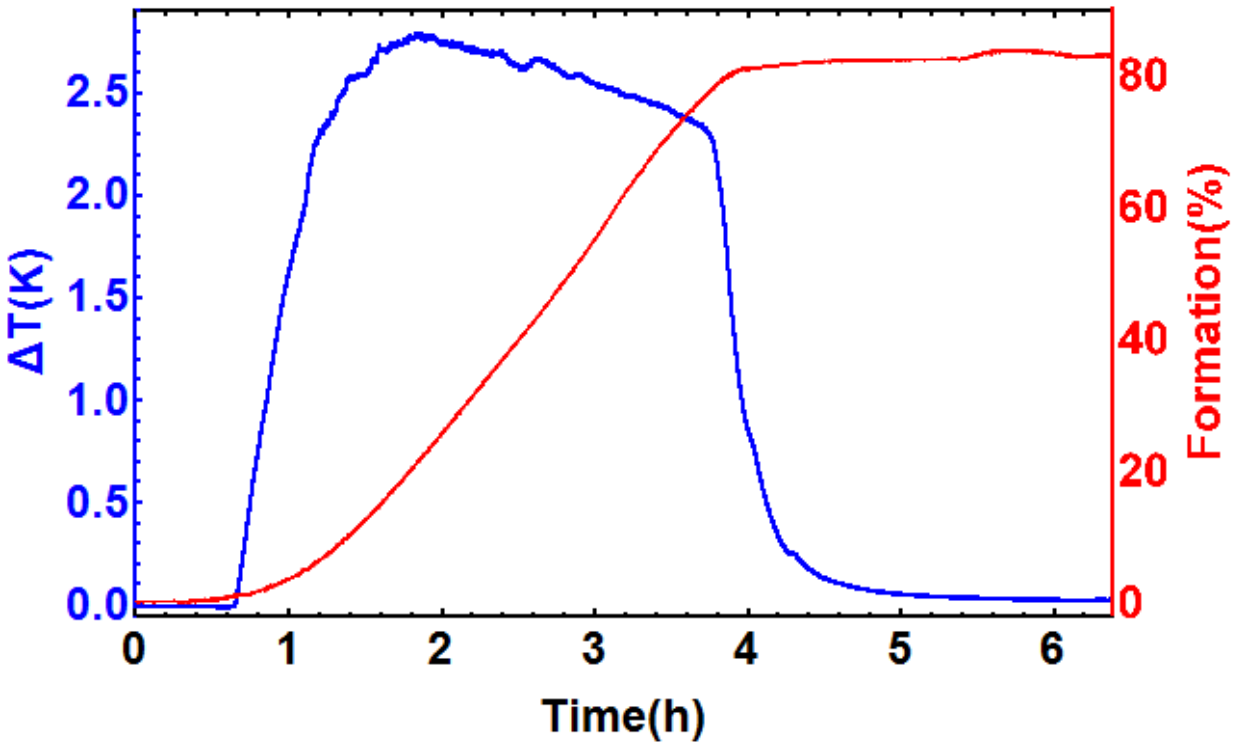

Figure 4.6: Temperature difference between the hydrate-forming water beaker and the main body of the pressure cell, alongside the methane absorbed as a percentage of the maximum possible.

beginning of hydrate formation (Figure 4.6). The temperature fell back down as formation levelled off. This spike is caused by the release of latent heat from hydrate formation.

Using a Savitzky-Golay filter to find a smoothed derivative of the water's temperature and applying Equation 3.3, we found the power due to latent heat as a function of time (Figure 4.7). To get the total heat released, we took a sum of the power with time, approximating an integral:

$$Q_{tot} = \sum_n \frac{\frac{1}{2}\{(\frac{dQ}{dt})_{n+1} + (\frac{dQ}{dt})_n\}}{t_{n+1} - t_n} \tag{4.1}$$

We thus found a total heat release of 11.66 kJ. Dividing this total energy by the amount of water converted to clathrate gave the latent heat of formation.

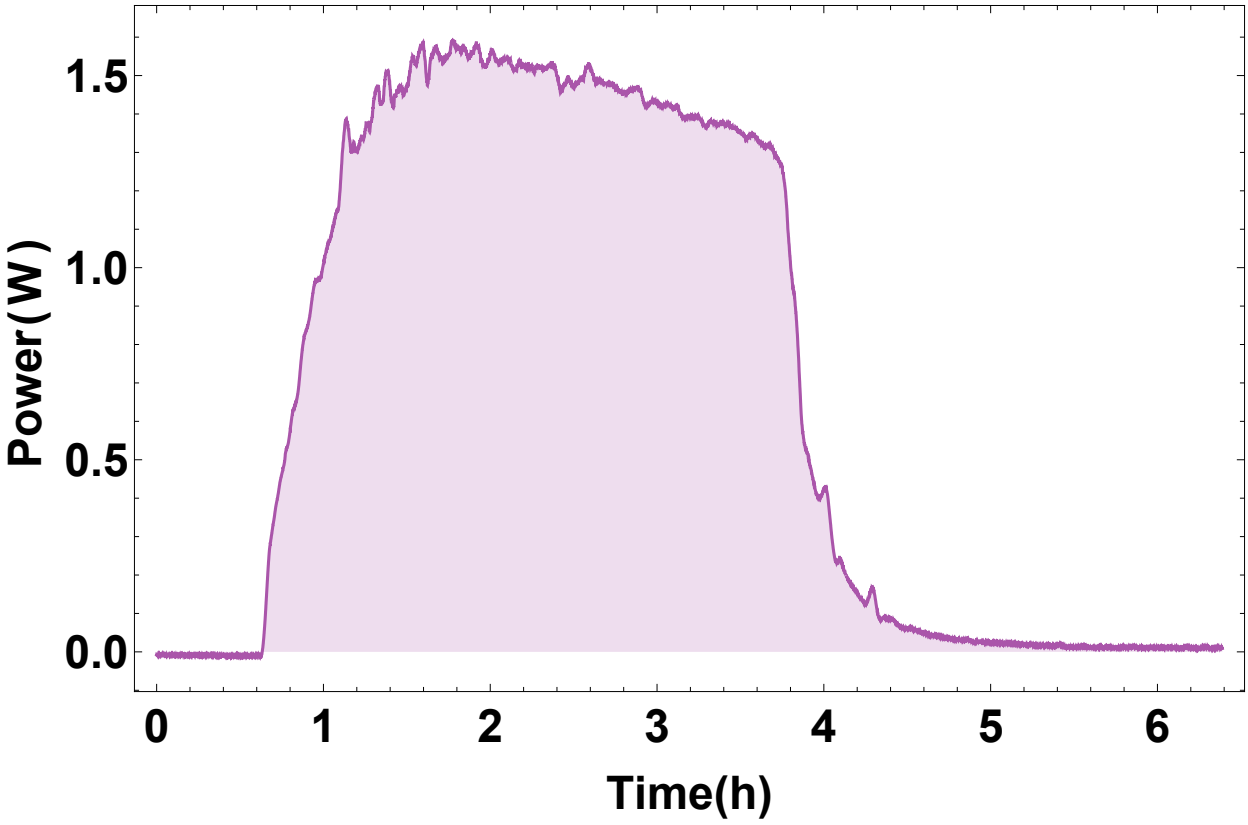

Figure 4.7: Power released by hydrate formation as a function of time, as given by Equation 3.3. Integrating gives the latent heat of formation.

$$L_{formation} = \frac{Q_{tot}}{m_w \frac{p_{tot}}{100\%}} \tag{4.2}$$

Since we used $m_w = 40$ grams of water and the final clathration amount was $p_{tot} = 82.9\%$, we determined the latent heat to be 486 J/g.

We made measurements of the latent heat of fusion of deionized water using the same procedure in order to test our apparatus. We determined it to be 291 J/g.

Chapter 5

Conclusion

We measured the latent heat of formation for deionized water containing sodium dodecyl sulfate. Our latent heat of formation result of 486 J/g = 60.3 kJ/mol is in agreement with values calculated by the Clapeyron equation and through dissociation experiment[31] of 56.9 kJ/mol and 54.2 kJ/mol, respectively. Our latent heat of fusion result for water was 291 J/g, in agreement with the literature value of 334 J/g.

We measured formation rates (normalized with driving force) and total hydrate formation amounts for solutions containing 0%, 0.1 wt%, 0.5 wt %, 1 wt%, 3.5 wt%, 5 wt%, and 10 wt% NaCl in the presence of the the surfactants sodium dodecyl sulfate, potassium dodecyl sulfate, and sodium laurate in most combinations. We found that both the formation rate and total amount of hydrate formed dropped steeply when NaCl concentration is increased. Total formation amounts dropped to around $^1/_4$, and normalized growth rates dropped to less than $^1/_{16}$ of their 0 wt% value in a 10 wt% NaCl solution. This indicates that, in addition to acting as a thermodynamic inhibitor, NaCl acted as a kinetic inhibitor to hydrate growth in these systems. NaL seemed to outperform the other two surfactants in terms of total formation and growth rate at low NaCl concentrations.

Points of comparison in the literature are scarce. There have been few experiments on growth kinetics in systems containing salts, and none in quiescent systems utilizing surfactants. Mekala et al.[1] grew methane hydrates from 3.03 wt% NaCl seawater in silica sand and observed a sharper decrease than we did, with a decrease by a factor of six versus pure water compared to our decrease by a factor of $\sim$2.7. Chong et al.[2] also grew methane hydrates in silica sand, with NaCl concentrations of 1.5 wt% and 3 wt%, and observed a smaller decrease with a reduction by a factor of $\sim$1.5. More research is clearly required in this area to better understand these kinetic effects.

Bibliography

[1] Prathyusha Mekala, Ponnivalavan Babu, Jitendra S. Sangwai, and Praveen Linga. Formation and Dissociation Kinetics of Methane Hydrates in Seawater and Silica Sand. *Energy & Fuels*, 28(4):2708–2716, apr 2014.

[2] Zheng Rong Chong, Adeline Hui Min Chan, Ponnivalavan Babu, Mingjun Yang, and Praveen Linga. Effect of NaCl on methane hydrate formation and dissociation in porous media. *Journal of Natural Gas Science and Engineering*, 27:178–189, nov 2015.

[3] Y. Zhong and R.E. Rogers. Surfactant effects on gas hydrate formation. *Chemical Engineering Science*, 55(19):4175–4187, oct 2000.

[4] J. S. Zhang, Sangyong Lee, and Jae W. Lee. Kinetics of Methane Hydrate Formation from SDS Solution. *Industrial & Engineering Chemistry Research*, 46(19):6353–6359, sep 2007.

[5] Kazunori Okutani, Yui Kuwabara, and Yasuhiko H. Mori. Surfactant effects on hydrate formation in an unstirred gas/liquid system: An experimental study using methane and sodium alkyl sulfates. *Chemical Engineering Science*, 63(1):183–194, jan 2008.

[6] J. L. De Roo, C. J. Peters, R. N. Lichtenthaler, and G. A. M. Diepen. Occurrence of methane hydrate in saturated and unsaturated solutions of sodium chloride and water in dependence of temperature and pressure. *AIChE Journal*, 29(4):651–657, jul 1983.

[7] P. Englezos and P. R. Bishnoi. Prediction of gas hydrate formation conditions in aqueous electrolyte solutions. *AIChE Journal*, 34(10):1718–1721, oct 1988.

[8] M.D Jager and E.D Sloan. The effect of pressure on methane hydration in pure water and sodium chloride solutions. *Fluid Phase Equilibria*, 185(1-2):89–99, jul 2001.

[9] H. Davy. The Bakerian Lecture: On Some of the Combinations of Oxymuriatic Gas and Oxygene, and on the Chemical Relations of These Principles, to Inflammable Bodies, 1811.

[10] M. Faraday and H. Davy. On Fluid Chlorine, 1823.

[11] E. G. Hammerschmidt. Formation of Gas Hydrates in Natural Gas Transmission Lines. *Industrial & Engineering Chemistry*, 26(8):851–855, aug 1934.

[12] J.P. Lederhos, J.P. Long, A. Sum, R.L. Christiansen, and E.D. Sloan. Effective kinetic inhibitors for natural gas hydrates. *Chemical Engineering Science*, 51(8):1221–1229, apr 1996.

[13] JH Van der Waals and JC Platteeuw. Clathrate solutions. *Advances in Chemical ...*, 1958.

[14] G. A. Jeffrey. Hydrate inclusion compounds. *Journal of Inclusion Phenomena*, 1(3):211–222, 1984.

[15] M. v. Stackelberg and H. R. Müller. Zur Struktur der Gashydrate. *Naturwissenschaften*, 38(19):456–456, jan 1951.

[16] John A. Ripmeester, John S. Tse, Christopher I. Ratcliffe, and Brian M. Powell. A new clathrate hydrate structure. *Nature*, 325(6100):135–136, jan 1987.

[17] Craig J. Taylor, Kelly T. Miller, Carolyn A. Koh, and E. Dendy Sloan. Macroscopic investigation of hydrate film growth at the hydrocarbon/water interface. *Chemical Engineering Science*, 62(23):6524–6533, dec 2007.

[18] AL Ballard and ED Sloan. The next generation of hydrate prediction: an overview. *Journal of Supramolecular Chemistry*, 2002.

[19] Naoki Ando, Yui Kuwabara, and Yasuhiko H. Mori. Surfactant effects on hydrate formation in an unstirred gas/liquid system: An experimental study using methane and micelle-forming surfactants. *Chemical Engineering Science*, 73:79–85, may 2012.

[20] Dirk D Link, Edward P Ladner, Heather A Elsen, and Charles E Taylor. Formation and dissociation studies for optimizing the uptake of methane by methane hydrates. *Fluid Phase Equilibria*, 211(1):1–10, aug 2003.

[21] M Albertí, A Costantini, A Laganá, and F Pirani. Are micelles needed to form methane hydrates in sodium dodecyl sulfate solutions? *The journal of physical chemistry. B*, 116(14):4220–7, apr 2012.

[22] Kazuyoshi Watanabe, Shuntaro Imai, and Yasuhiko H. Mori. Surfactant effects on hydrate formation in an unstirred gas/liquid system: An experimental study using HFC-32 and sodium dodecyl sulfate. *Chemical Engineering Science*, 60(17):4846–4857, sep 2005.

[23] P. Gayet, C. Dicharry, G. Marion, A. Graciaa, J. Lachaise, and A. Nesterov. Experimental determination of methane hydrate dissociation curve up to 55MPa by using a small amount of surfactant as hydrate promoter. *Chemical Engineering Science*, 60(21):5751–5758, nov 2005.

[24] Dennis Elwell and Hans J. Scheel. Crystal growth from high-temperature solutions. 2011.

[25] E. Dendy Sloan, Jr., and Carolyn Koh. *Clathrate Hydrates of Natural Gases, Third Edition*. CRC Press, 2007.

[26] P. Englezos, N. Kalogerakis, P.D. Dholabhai, and P.R. Bishnoi. Kinetics of formation of methane and ethane gas hydrates. *Chemical Engineering Science*, 42(11):2647–2658, jan 1987.

[27] Ding-Yu Peng and Donald B. Robinson. A New Two-Constant Equation of State. *Industrial & Engineering Chemistry Fundamentals*, 15(1):59–64, feb 1976.

[28] M. Frenkel Director Thermodynamics Research Center, NIST Boulder Laboratories. Thermodynamics Source Database. In *NIST Chemistry WebBook, NIST Standard Reference Database Number 69*, chapter Thermodyna. 2016.

[29] U. Setzmann and W. Wagner. A New Equation of State and Tables of Thermodynamic Properties for Methane Covering the Range from the Melting Line to 625 K at Pressures up to 100 MPa. *Journal of Physical and Chemical Reference Data*, 20(6):1061, nov 1991.

[30] Abraham. Savitzky and M. J. E. Golay. Smoothing and Differentiation of Data by Simplified Least Squares Procedures. *Analytical Chemistry*, 36(8):1627–1639, jul 1964.

[31] E. Dendy Sloan and Jr. *Clathrate Hydrates of Natural Gases, Second Edition, Revised and Expanded*. CRC Press, 1998.